Expanded View Figures

Figure EV1. Resolution and quality of the cryo-EM reconstructions.

A–C Surface rendering of the final high-resolution maps of the 30S subunit (A), the 70S ribosome (B) and the 50S subunit (C).

D–I Local resolution plots showing the surface (D–F) and a cross section (G–I) of the cryo-EM maps. Local resolution maps of the 30S (D, G), 70S (E, H) and 50S (F, I) are shown from the same view as in panels (A, B and C), respectively.

J–L Fourier shell correlation (FSC) curves of the 30S (J), the 70S (K) and 50S (L) cryo-EM reconstructions. The indicated resolutions are according to the FSC = 0.143 criterion ("gold-standard").

M–O Examples for the quality of the density: (M) ribosomal protein (salmon) interacting with rRNA (grey), (N) protein α-helix (yellow) and (O) protein β-sheet (green).

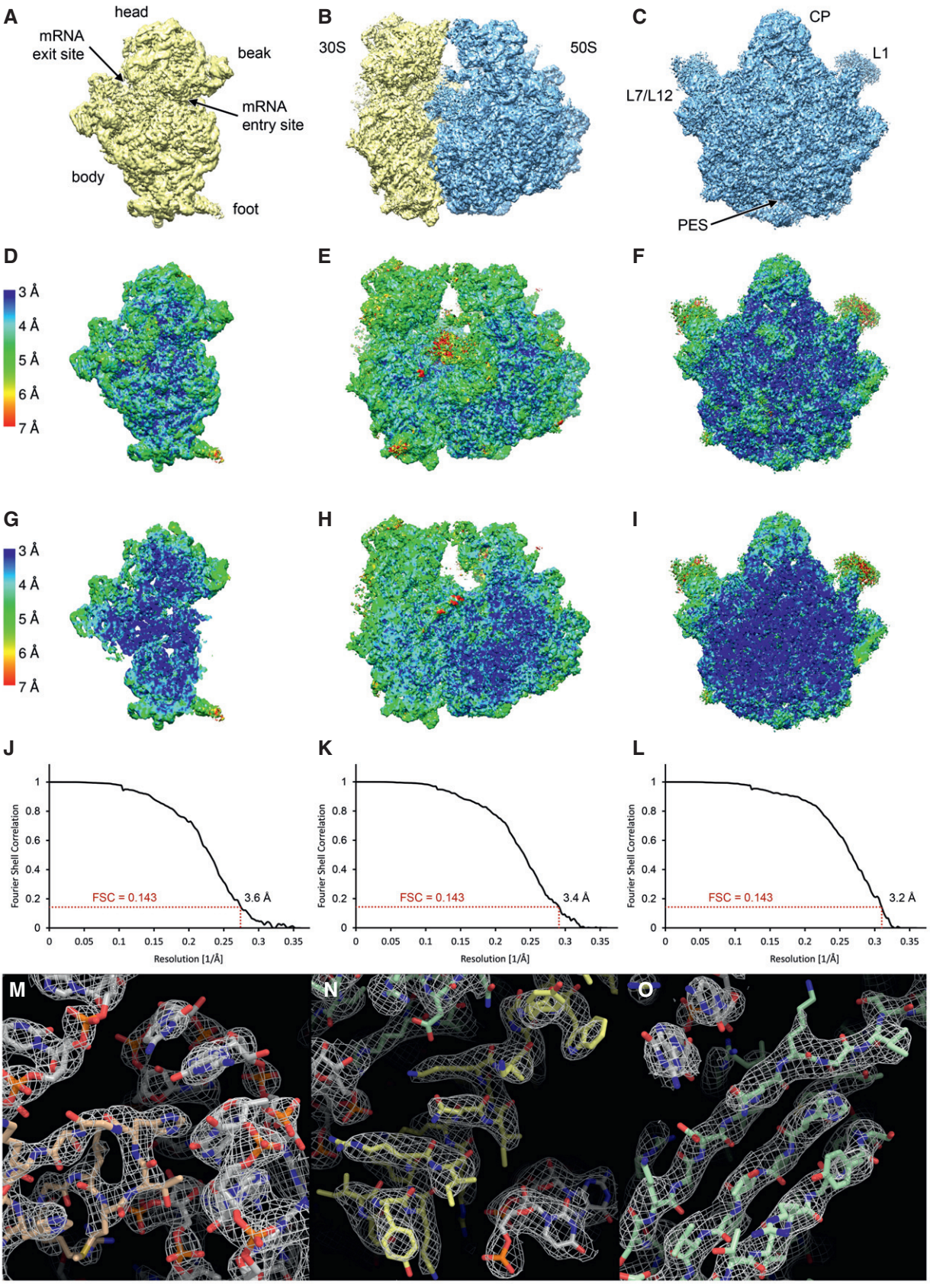

Figure EV1.

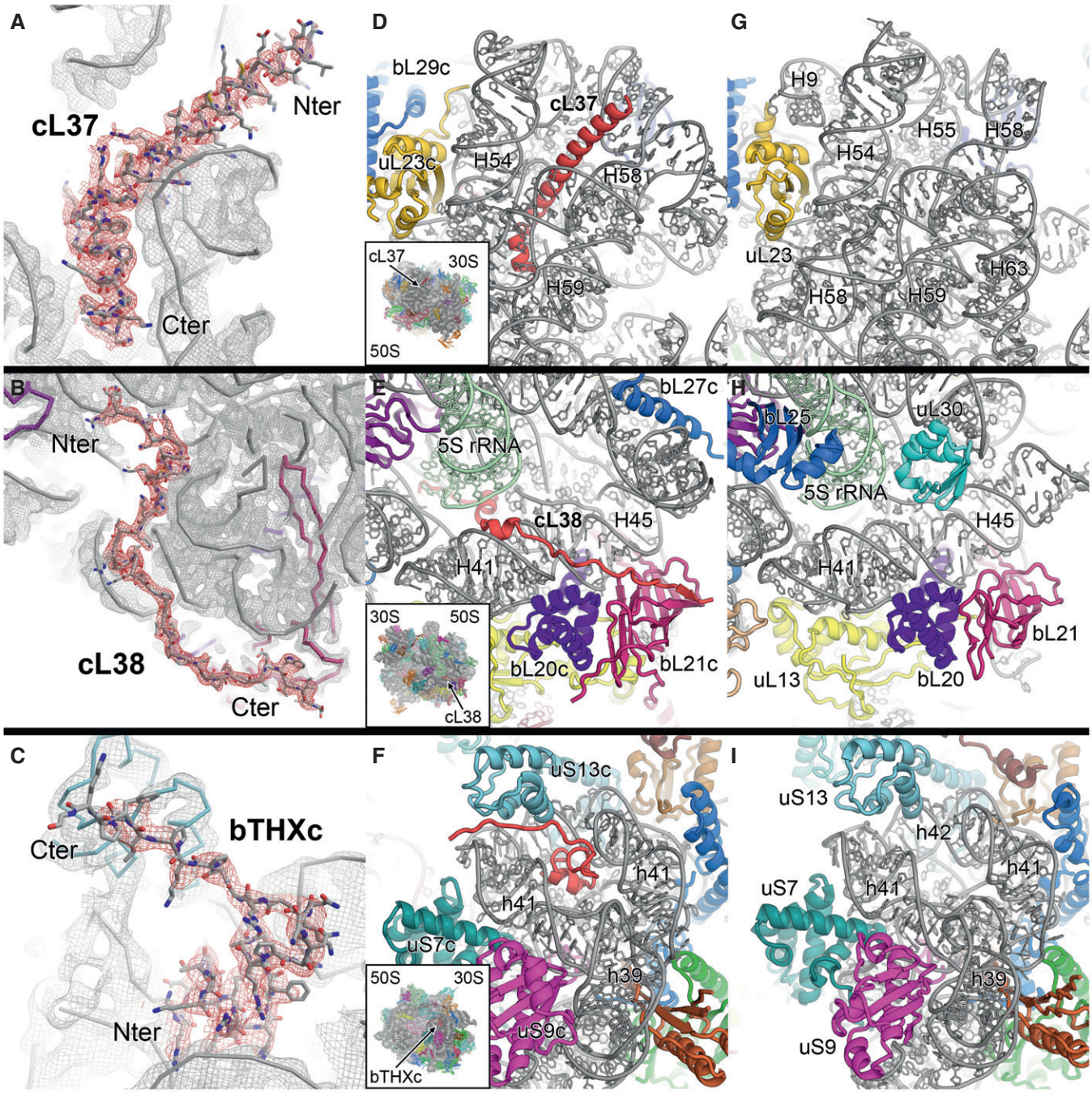

Figure EV2. *De novo* built plastid-specific ribosomal proteins.

A–C The density indicates clear side chain features and allows unambiguous tracing of cL37 (A), cL38 (B) and bTHXc (C).

D–F Binding sites of cL37 (D), cL38 (E) and bTHXc (F) in the chloroplast 70S ribosome.

G–I Corresponding sites to panels (D, E and F), respectively, in the bacterial 70S ribosome (PDB 4YBB; Noeske *et al*, 2015).

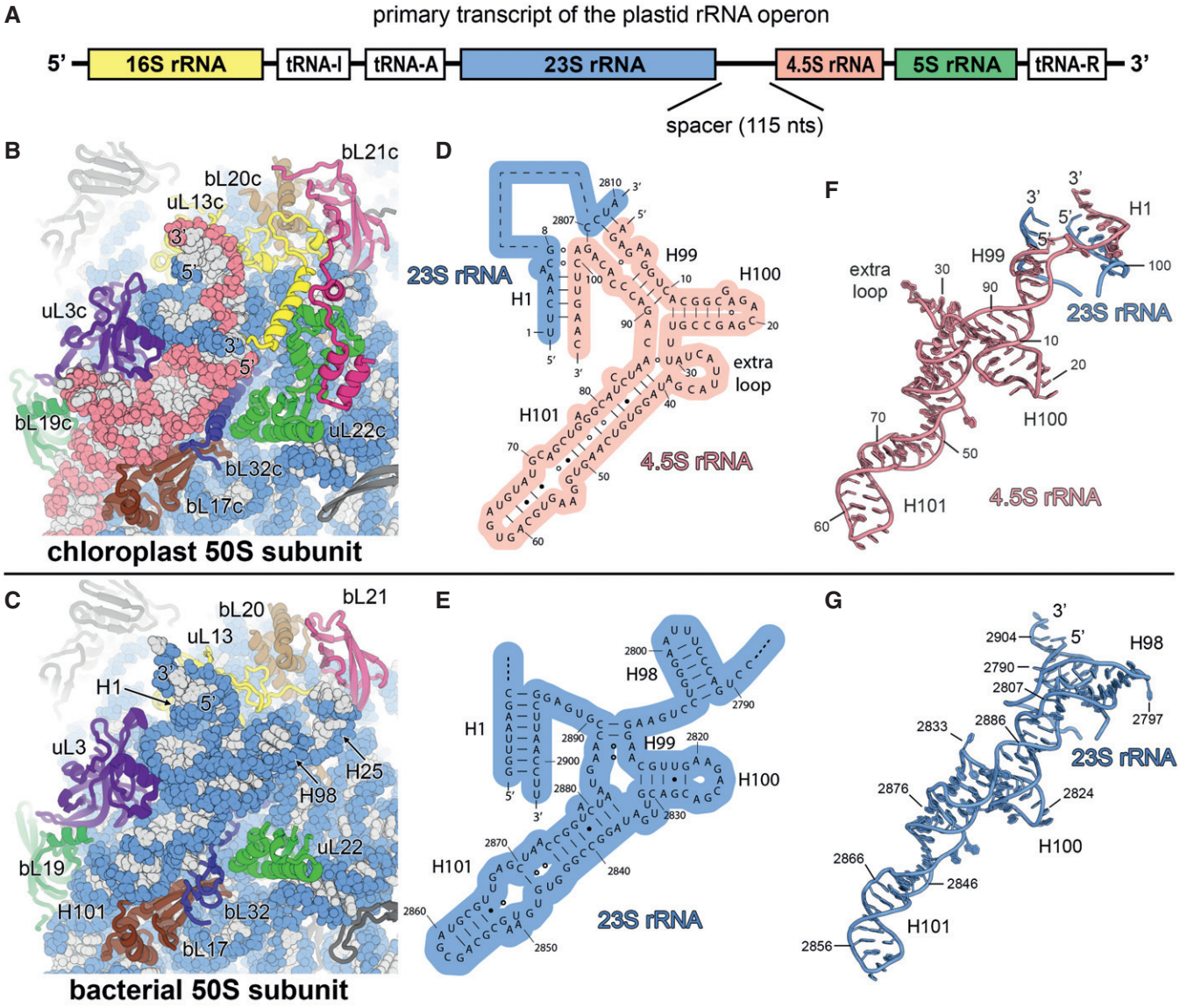

Figure EV3. The chloroplast 4.5S ribosomal RNA.

A Primary transcript of the chloroplast rRNA operon. The canonical sequences of ribosomal RNAs are indicated by coloured boxes. The 4.5S rRNA is separated from the 23S rRNA by a 115-nucleotide RNA spacer.

B, C Comparison of the chloroplast 50S subunit (B) with the bacterial 50S subunit (PDB 4YBB; Noeske *et al*, 2015) (C) indicating the structural rearrangement of the ribosomal proteins that interact with the 23S rRNA (blue) and the 4.5S rRNA (red).

D, E Secondary structure diagram of the chloroplast 4.5S rRNA (D) and the 3′ end of the bacterial 23S rRNA (E). The interactions of the 5′ and 3′ ends of the 4.5S rRNA with the 23S rRNA are shown. Watson–Crick base pairs are indicated by lines (-), G•U base pairs by dots (•) and non-standard base pairs by rings (○).

F, G Model of the chloroplast 4.5S rRNA (F) and the 3′ end of the bacterial 23S rRNA (G). The same nucleotides are shown in the models as represented in the secondary structure diagrams (D, E).

Figure EV4. The hidden breaks of the 23S rRNA.

A Analysis of ribosomal RNA by agarose gel electrophoresis. RNA was extracted from chloroplast 70S ribosome sample and separated on a 2% (w/v) agarose gel (L: high range RNA ladder; 70S: RNA of chloroplast 70S sample).

B Schematic of rRNA processing and assembly in the chloroplast. Because of two specific cleavage sites on the 23S rRNA, called "hidden breaks", the 23S rRNA gets separated into three fragments: A (0.5 kb), B (1.2 kb) and C (1.1 kb).

C–E Views of the 30S (C) and the 50S subunits (D) from the subunit interface and of the 50S subunit (E) from the solvent accessible side. The rRNA is shown as spheres and coloured according to the elements indicated in panel (B). The positions of the hidden breaks on the 23S rRNA are marked with triangles.

F–H The hidden break indicated with a triangle between fragments A and B is introduced in the connection between helices H2 and H24.

I–K The hidden break indicated with a triangle between fragments B and C is positioned at the stem loop of helix H63. The binding site of the helicase RH39 on helix H62 is coloured black. The electron density map shown in panels (H and K) is low-pass filtered to 4 Å, and the nucleotides at the hidden break sites are labelled. The exact positions of the hidden breaks on the 23S rRNA sequence shown in panels (F and I) were stated in a previous publication (Liu *et al*, 2015).

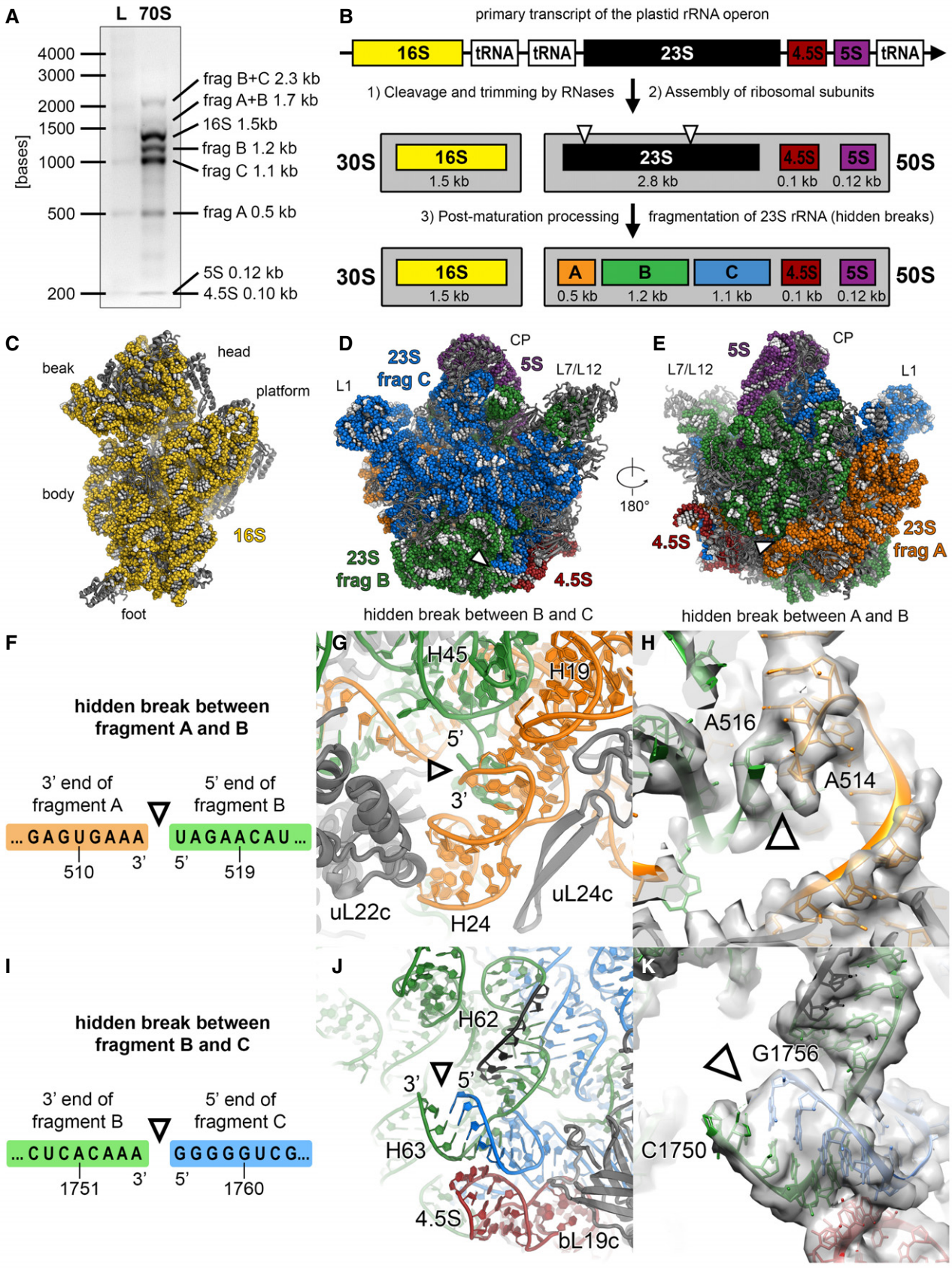

Figure EV4.

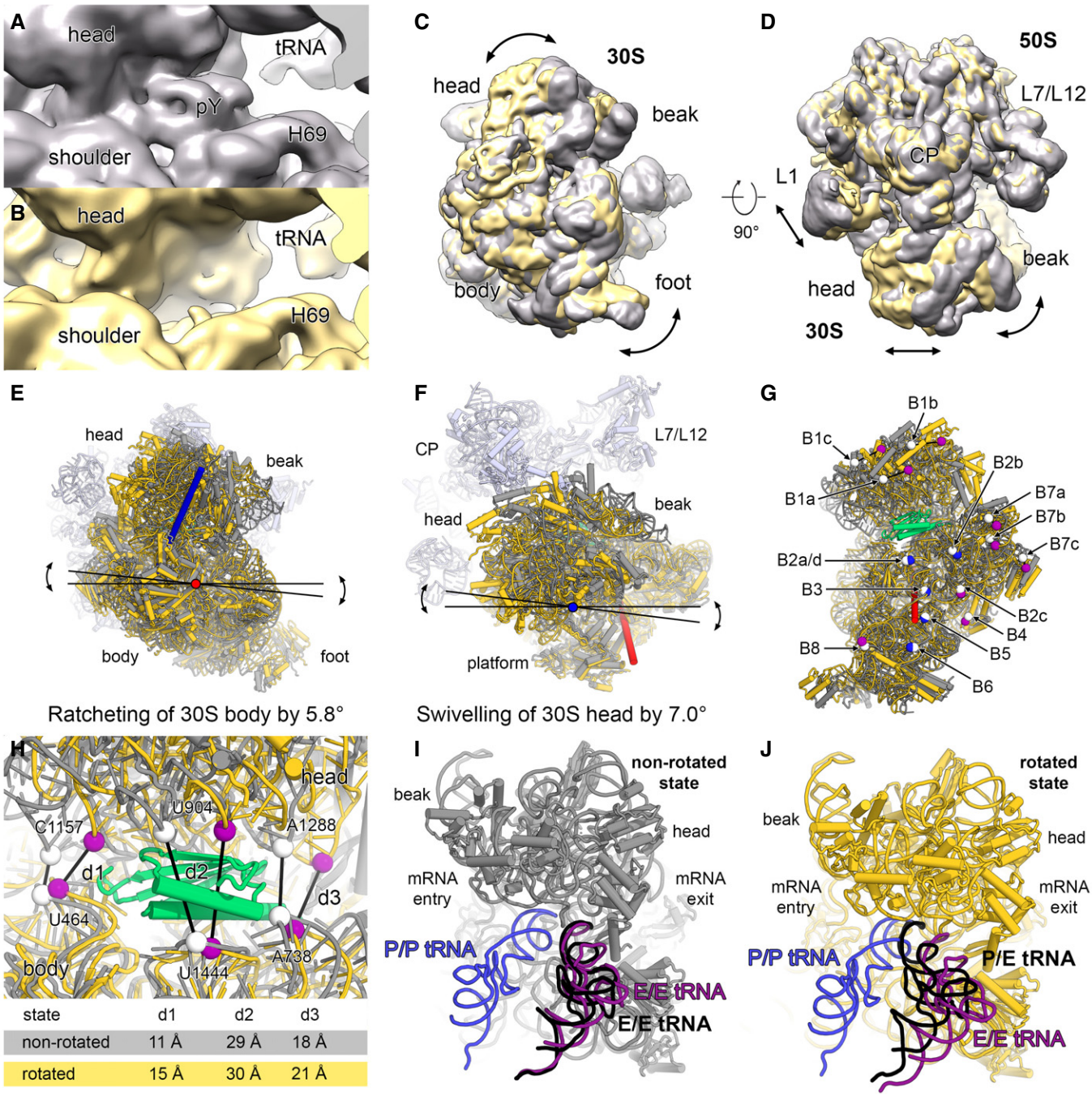

state	d1	d2	d3
non-rotated	11 Å	29 Å	18 Å
rotated	15 Å	30 Å	21 Å

Figure EV5. Plastid translation factor pY.

A–D The 70S map with density for pY in the mRNA channel is shown in grey (A) and the empty 70S map is shown in yellow (B). The 70 maps were overlaid using only the density of the 50S. Comparison of the overlaid maps, shown in 30S subunit view (C) and top view (D). The rotation of the 30S subunit is indicated with arrows.

E, F The body and the head domains of the 30S model were independently fitted into the cryo-EM map of the rotated state. The rotation angle of the 30S body rotation (ratcheting) (E) and the 30S head rotation (swivelling) (F) were measured using PyMOL, and the rotation axes are shown in red and blue, respectively.

G Intersubunit bridges are affected by the 30S rotation. A selected residue of each intersubunit bridge is represented as white sphere in the non-rotated state. The same residues are coloured in the rotated state either in blue, if the contact with the large subunit is maintained, or in purple, if the contact is lost. The intersubunit bridges and the differences between the rotated and the non-rotated state are described in Appendix Table S4.

H Distances (d1, d2 and d3) between backbone phosphates of selected rRNA residues (spheres) in the non-rotated (white) and the rotated state (purple) indicating a slight opening of the mRNA channel.

I, J tRNAs in the P/P- and E/E-state from a crystal structure of the bacterial 70S ribosome in complex with mRNA and tRNAs (PDB 4V51; Selmer *et al*, 2006) are overlaid and shown in blue and purple, respectively. A tRNA (black) was fitted as rigid body into the 70S maps of the non-rotated (I) and of the rotated state (J).